I&EC research
Industrial & Engineering Chemistry Research

pubs.acs.org/IECR

Article

Reaction Kinetics and Microenvironments between Alkylimidazole and Methylthiocyanate for the Synthesis of Ionic Liquids

Weizhong Zheng, Fan Zhang, Fan Yang, Weizhen Sun,* and Ling Zhao*

Cite This: *Ind. Eng. Chem. Res.* 2023, 62, 14963−14972

Read Online

ACCESS | Metrics & More | Article Recommendations | Supporting Information

ABSTRACT: The alkyl chain length of the alkylimidazole nucleophile plays an important role in the reaction and microenvironment behaviors for the synthesis of imidazolium-based ionic liquids with different alkyl chain lengths. Herein, the reaction kinetics and microenvironments between alkylimidazole (MIm, EIm, and BIm) and methylthiocyanate (MeSCN) were investigated to reveal the effects of the alkyl chain length of the imidazole nucleophile on the synthesis of the imidazole-based ILs using time-dependent Fourier transform infrared (FTIR) spectra and classical molecular dynamics (MD) simulations. Experimental results indicate that the BIm/MeSCN system shows a smaller reaction rate constant compared to the EIm/MeSCN system and MIm/MeSCN system, and an alkylimidazole nucleophile with a longer alkyl chain leads to a higher activation energy. MD simulations show that MeSCN possesses a decreased distribution near the alkyl chain and an increased distribution around the N atom with isolated electrons of alkylimidazole with a prolonged alkyl chain. In addition, the diffusion and reorientation dynamics of both alkylimidazole and MeSCN are slowed in the system with the longer-alkyl-chain alkylimidazole, which also contributes to the slower reaction rate. This work will provide a better understanding of the reaction and microenvironment behaviors to guide the synthesis of ILs with different alkyl chains.

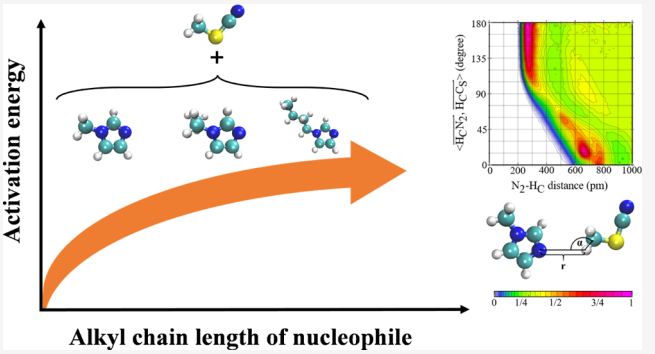

1. INTRODUCTION

Ionic liquids (ILs) are defined as a material consisting of only ionic species with a melting point lower than the ambient temperature. As the next great class of environmentally friendly solvents/catalysts, ILs are becoming increasingly prevalent in a wide range of fields and applications, such as catalysis, extraction, and separation,[1,2] owing to the negligible vapor pressure, high ionic conductivity, large temperature stability, and good solvent properties.[3−5] The alkyl chain lengths of the cations in ionic liquids (ILs) play a crucial role in determining their physicochemical properties. The investigations related to the effect of the alkyl chain length of imidazolium (alkylimidazolium) cations on the properties of imidazolium-based ILs have attracted considerable attention, including density, polarizability, surface tension, conductivity, nano-segregation, diffusion, and thermal stabilities.[6−12] The combination of cations and anions can adjust the properties for the targeted applications.[13,14] However, the synthesis of ILs is usually carried out in a batch way without the known kinetics and takes an empirically long reaction time, especially for the ILs with long alkyl chain,[15,16] which results in little emphasis on the reaction process intensification from the point of industrial view.

The ILs are prepared according to the well-known Menshutkin S_N2 reaction; that is, two so-called neutral nucleophile and substrate reactants generate a transition state with significant charge separation and then form a full charge separation in the product with cations and anions. As for the reaction kinetics, the preparation of 1-hexyl-3-methylimidazoline bromide in different solvents was studied in detail with emphasis on the reaction kinetics and solvent effects.[17] The reaction kinetics between ethylmethylimidazole and ethylsulfate was investigated based on the different reactor types.[18] Although the synthesis of pyrrolidinium- and imidazolium-based ILs with different alkyl chain lengths was conducted, the corresponding reaction kinetics was not focused on.[16,19] In our recent work, the reaction kinetics and microdynamics between 1-methylimidazole (MIm) nucleophile and alkylthiocyanate substrate (RSCN, R = methyl, ethyl, and butyl groups) for the preparation of imidazolium-based ILs with different alkyl chain lengths were analyzed by time-dependent Fourier transform infrared (FTIR) spectra and classical molecular dynamics (MD) simulation. It is found that the longer chain length of the thiocyanate substrate leads to a significantly smaller

Received: May 5, 2023
Revised: August 20, 2023
Accepted: August 22, 2023
Published: September 5, 2023

https://doi.org/10.1021/acs.iecr.3c01512
Ind. Eng. Chem. Res. 2023, 62, 14963−14972

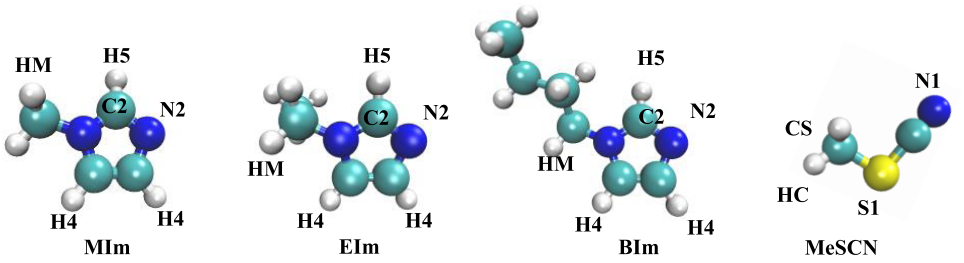

Figure 1. Optimized molecular structures of MIm, EIm, BIm, and MeSCN are shown with atom labels.

reaction rate constant with a higher activation energy. For example, the activation energies of the MIm/BuSCN system are increased by 27.5 kJ/mol compared to that of the MIm/MeSCN system. MD simulations indicate that the long alkyl chain of thiocyanate results in a weaker spatial distribution of reaction sites as well as slower diffusion and reorientation, which can reduce the intermolecular collision probability.[20] The imidazolium-based ILs with the same alkyl substituents can also be synthesized by the low-cost alkylimidazole nucleophile and MeSCN substrate, which motivates us to further probe the reaction kinetics and microenvironments between alkylimidazole and MeSCN with emphasis on the imidazole nucleophile with different alkyl chain lengths.

MD simulation can act as a promising and effective tool to probe the complex microscopical structure and dynamics behaviors, which has been extensively used to reveal the physicochemical properties of alkylimidazolium-based IL-related systems at the molecular level.[21−24] For instance, the density, diffusion coefficient, vaporization enthalpy, reorientation correlation time, and viscosity of ILs consisting of 1-alkyl-3-methylimidazole cations and bis(trifluoromethylsulfonylimine) anions ($[C_nMIm][NTf_2]$, n = 2, 4, 6, 8) were systemically investigated.[22] The microstructure of the 1-ethyl-3-methylimidazole acetate and water mixtures at different water contents was studied by calculating the structure, hydrogen bonding, characteristic bond length, and angles of cations and anions.[25] The structure of the alkylimidazolium-based IL at the interface with vacuum and water was also studied, in which various physical properties are calculated and validated against experimental values. It is observed that ILs with short alkyl chains orient at the surface, while ILs with longer chains orient with alkyl chains protruding into the vacuum at the IL/vacuum interface and into the bulk IL at the IL/water interface.[26] Nevertheless, there are few reports to address the microscopic structure, dynamics, and reaction behaviors that affect the reaction kinetics of the imidazole nucleophile with different alkyl chain lengths for the synthesis of ILs.

In addition, the ionic liquids with thiocyanate-based anion show important applications in the extraction of model oils for deep desulfurization,[27] separation of cresols from coal tar,[28] and as corrosion inhibitors for steel.[29] Therefore, in this work, the effects of the alkyl chain length of the imidazole nucleophile on reaction kinetics and microenvironments between the alkylimidazole (MIm, EIm, and BIm) nucleophile and MeSCN substrate were investigated using in situ FTIR and MD simulations. The reaction rate constants and reaction activation energies were obtained by FTIR characterization, and the increase in the alkyl chain length of the imidazole nucleophile contributes to the reduced reaction rate and larger activation energy. MD simulations suggest that the longer alkyl chain of imidazole renders a higher distribution of MeSCN around the reaction-activated sites of alkylimidazole. However, slower diffusion and reorientation dynamics of the reaction system were observed with an increased alkyl chain length of the imidazole nucleophile, which plays a fundamental role in the decreased reaction rate.

2. EXPERIMENTAL AND MD DETAILS

2.1. Sample Preparation. Alkylimidazole (MIm, EIm, and BIm) nucleophiles and methylthiocyanate (MeSCN) substrate reactants with a 20:1 molar ratio were mixed in the scintillation vial in a glovebox to prevent air humidity. After 5 min of stirring, the sample was charged into the FTIR sample cell with a CaF_2 window. The FTIR spectra were recorded every 15 min for an initial 4 h at the given temperature. Then, the sample was heated to 360 K in a glovebox until the reaction was completed. At the same time, the FTIR spectra were recorded every day. The fractional yields of SCN^- were calculated by the resulting time-dependent spectra of the CN stretching mode.[30]

2.2. Reaction Rate Calculation. The reaction was between MeSCN with alkylimidazole (MIm, EIm, and BIm) to form the ionic liquid 3-alkyl-1-methylimidazolium thiocyanate (RMImSCN). Here, we give the reaction between MIm and MeSCN, for example

$$\mathrm{MIm} + \mathrm{MeSCN} \xrightarrow{k_1} \mathrm{MMIm}^+ + \mathrm{SCN}^- \tag{1}$$

The rate-limiting step depends on the concentrations of MIm and MeSCN, following the second-order reaction kinetics

$$\text{rate} = k_1[\mathrm{MIm}][\mathrm{MeSCN}] \tag{2}$$

where k_1 is the forward rate constant with units M^{-1} s^{-1}.

In the 1:20 MeSCN/MIm mixture, MIm was used in excess, and thus MIm remains approximately constant over the whole reaction process, particularly at an early time. Thus, eq 2 can be approximated as a pseudo-first-order reaction

$$\text{rate} = k[\mathrm{MeSCN}] \tag{3}$$

where $k = k_1[\mathrm{MIm}]$. Rewritten in terms of $[SCN^-]$

$$\text{rate} = \frac{\mathrm{d}[\mathrm{SCN}^-]}{\mathrm{d}t} = k([\mathrm{MeSCN}]_i - [\mathrm{SCN}^-]) \tag{4}$$

where $[\mathrm{MeSCN}]_i$ is the initial MeSCN concentration. The solution to eq 4 is

$$[\mathrm{SCN}^-] = [\mathrm{MeSCN}]_i(1 - \mathrm{e}^{-kt}) \tag{5}$$

Thus, the rate constant k can be calculated by monitoring the formation of the SCN^- product as a function of time. The CN stretching vibration of SCN^- can be monitored through FTIR spectroscopy. The CN stretch band area, A_{SCN^-}, is related to $[SCN^-]$ through Beer's law

https://doi.org/10.1021/acs.iecr.3c01512
Ind. Eng. Chem. Res. 2023, 62, 14963−14972

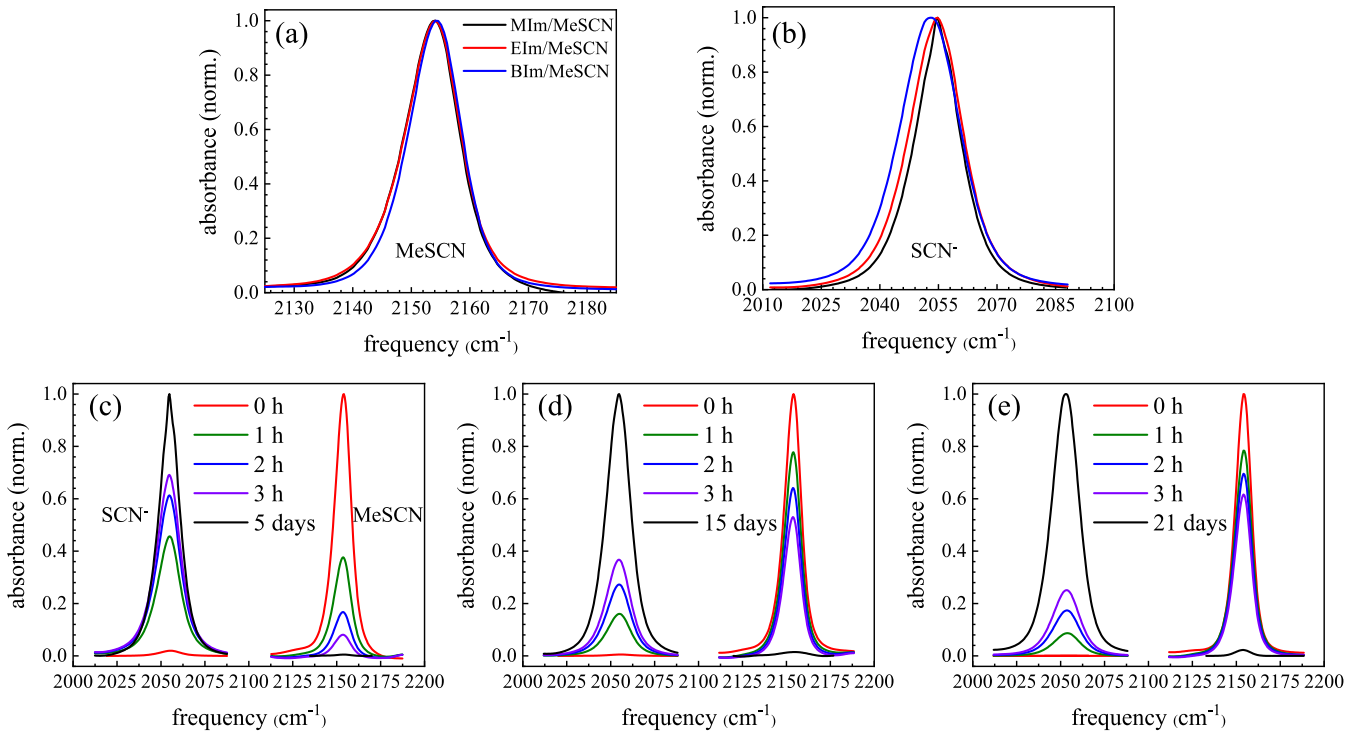

Figure 2. Normalized background-subtracted FTIR spectra of the CN stretching mode of MeSCN (a) and SCN^- (b) and time-dependent normalized and background-subtracted FTIR spectra of (c) MIm/MeSCN, (d) EIm/MeSCN, and (e) BIm/MeSCN systems at 340 K.

$$A_{SCN^-}(t) = l\int \varepsilon(\omega)c(\omega, t)\mathrm{d}\omega$$
$$[SCN^-] = \int c(\omega, t)\mathrm{d}\omega \quad (6)$$

where l is the sample path length, and $\varepsilon(\omega)$ and $c(\omega, t)$ are the frequency-dependent extinction coefficient and SCN^- concentration, respectively. When the reaction is complete, $[SCN^-]_f = [MeSCN]_i$. Thus

$$[SCN^-] = [MeSCN]_i \frac{A_{SCN^-}(t)}{A_{SCN^-}(t \to \infty)} \quad (7)$$

To simplify the determination of the rate constant, k, we analyzed the short time behavior of eq 5. When combined with eq 7, this gives the fractional yield of SCN^- as

$$\frac{[SCN^-]}{[MeSCN]_i} = \frac{[SCN^-]}{[SCN^-]_f} = \frac{A_{SCN^-}(t)}{A_{SCN^-}(t \to \infty)} \approx kt \quad (8)$$

2.3. MD Details. Figure 1 plots the optimized structures of MIm, EIm, BIm, and MeSCN. For MD simulations, the number of alkylimidazole and MeSCN molecules were 400 and 20, respectively, which was built using Packmol software.[31] The box sizes of MIm/MeSCN, EIm/MeSCN, and BIm/MeSCN systems were 35.0 Å × 34.3 Å × 34.0 Å, 36.9 Å × 37.7 Å × 37.7 Å, and 41.2 Å × 41.7 Å × 43.0 Å, respectively. For the obtained boxes, energy minimization was initially run for 10000 steps to eliminate the unreasonable structure. The constant-volume (*NVT*) ensemble with the Nose−Hoover thermostat was conducted for 5 ns,[32,33] and the isobaric−isothermal (*NPT*) ensemble with the Parrinello−Rahman barostat was carried out for full equilibration.[34,35] The last 15 ns trajectories were used to analyze the microstructure and microdynamic properties of interest.

The interactions among MIm, EIm, BIm, and MeSCN were represented by the Lennard-Jones (L-J) potential in the form of the OPLS-AA force field. The force field parameters of MeSCN were taken directly from our previous work.[20] The optimized structures of MIm, EIm, BIm, and MeSCN were gained at the B3LYP/6-311G(d,p) level, and the ChelpG charges were refitted at the same level using the Gaussian 09 program.[36] The parameters of the force field were validated based on the simulated density in comparison to the experimental one with a deviation in the range of 5% for MIm, EIm, BIm, and MeSCN, respectively, as shown in Table S1 in the Supporting Information. All of the MD simulations were conducted with GROMACS software with a time step of 1 fs.[37,38] The Lorentz−Berthelot mixing rules were used with periodic boundary conditions in three dimensions. The long-range electrostatic interactions were treated by the particle mesh Ewald method with a cutoff radius of 1.2 nm. The initial velocities were randomly generated from the Maxwell−Boltzmann distribution. The LINCS algorithm was used to constrain the hydrogen atom-related covalent bonds.

3. RESULTS AND DISCUSSION

3.1. FTIR Spectrum. The normalized background-subtracted CN stretch vibrations of MeSCN and SCN^- and the time-dependent normalized spectrum of MeSCN and SCN^- for the three systems at a temperature of 340 K are shown in Figure 2. The MeSCN and SCN^- spectra were normalized based on their initial and final values, respectively. The band centers of MeSCN and SCN^- were consistent with the previous studies.[32] From Figure 2a,b, the alkyl chain length of imidazole has little effect on the MeSCN peak at 2154.1 cm^{-1}. However, the peak centers of the SCN^- in the MIm/MeSCN, EIm/MeSCN, and BIm/MeSCN systems are 2055.3, 2054.8, and 2052.9 cm^{-1}, respectively, which indicates the red

https://doi.org/10.1021/acs.iecr.3c01512
Ind. Eng. Chem. Res. 2023, 62, 14963−14972

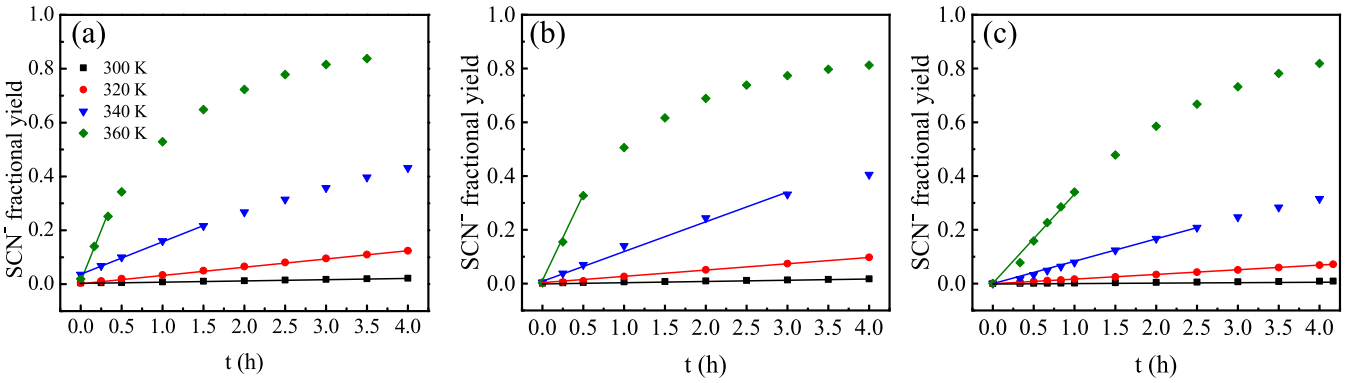

Figure 3. Time-dependent yield of SCN^- in (a) MIm/MeSCN, (b) EIm/MeSCN, and (c) BIm/MeSCN as a function of temperature. The dotted line is the experimental value, and the solid line represents the linear fitting.

Table 1. Temperature-Dependent Rate Constant and Activation Energies for Each System

	rate constants $k \times 10^2$ (h^{-1})					
systems	300 K	320 K	340 K	360 K	E_a (kJ/mol)	A (h^{-1})
MIm/MeSCN	0.452	2.840	11.585	38.119	66.3	1.67×10^9
EIm/MeSCN	0.340	2.146	9.132	33.411	68.4	2.95×10^9
BIm/MeSCN	0.222	1.729	8.759	32.267	74.6	2.35×10^{10}

shift of the peak center of SCN^- with increasing alkyl chain length. This is probably due to the charge delocalization of the longer-alkyl-chain imidazole cations with larger size, which causes the weaker hydrogen-bonding interaction between cations and anions and thus the red shift of the IR absorption peaks toward the lower frequencies.[39]

From Figure 2c–2e, the peak area of MeSCN gradually decreases, while the peak area of SCN^- increases during the reaction. Eventually, the MeSCN peak disappears completely, and the SCN^- peak reaches its maximum value, indicating that the reaction is almost over. The alkyl chain length of the alkylimidazole molecule affects the reaction time. For instance, the MIm/MeSCN system takes around 5 days to complete the reaction, while the BIm/MeSCN system requires approximately 21 days. These findings suggest that alkylimidazoles with longer alkyl chains contribute to a slower reaction rate, which can be attributed to the electronic properties and steric effects of the alkylimidazole molecules, which influence the reaction kinetics and product formation.

3.2. Rate Constant. The time-dependent fractional yields of SCN^- in the systems with different alkylimidazoles as a function of temperature were plotted, as shown in Figure 3. As expected, the elevated temperature leads to a faster reaction rate for all of the systems. For the systems related to the alkylimidazole with different alkyl chain lengths, the SCN^- yield in the MIm/MeSCN system reaches around 10% within 3 h at 320 K, while the SCN^- yield in the BIm/MeSCN system remains below 5% at the same conditions. Thus, it can be said that the longer alkyl chain of imidazole can result in a slower reaction rate, following the same trend as the alkylthiocyanate.[20]

The normalized peak area of SCN^- as a function of time within 4 h is plotted in Figure 3. Table 1 lists the rate constants (k) obtained from the slope of the fitting line based on pseudo-first order. The reaction rate constant of the MIm/MeSCN system increases by about 26 times from 300 to 340 K, which is consistent with the 25-fold increase in reaction rate for imidazolium-based ionic liquids from 298.2 to 333.2 K in the previously reported literature.[17] Within the temperature range studied, the rate constants of different systems decline with an increase in the alkyl chain length of imidazole. The rate constants of the EIm/MeSCN system and BIm/MeSCN system are about 1.3 times and 2 times lower than that of the MIm/MeSCN system at 300 K. Furthermore, the rate constants of the EIm/MeSCN system and the BIm/MeSCN system are about 1.1 times and 1.2 times lower than that of the MIm/MeSCN system at 360 K, respectively.

The rate constant of the thermal activation process with temperature can be described by the Arrhenius equation

$$k = A\, e^{-E_a/RT} \tag{9}$$

in which A, E_a, and R are the pre-exponential factor, the activation energy, and the ideal gas constant, respectively. The effect of the alkyl chain length of the imidazole nucleophile on the reaction activation energy is obtained by a plot of $\ln k$ versus $1/T$, as shown in Figure 4. The activation energies of the MIm/MeSCN, EIm/MeSCN, and BIm/MeSCN systems are 66.3, 68.4, and 74.6 kJ/mol, respectively, which indicates

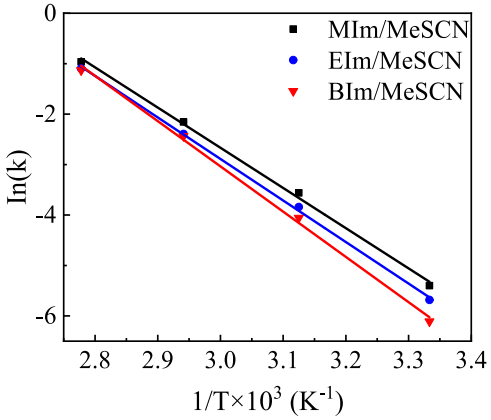

Figure 4. Arrhenius plots for MIm/MeSCN, EIm/MeSCN, and BIm/MeSCN systems.

https://doi.org/10.1021/acs.iecr.3c01512
Ind. Eng. Chem. Res. 2023, 62, 14963–14972

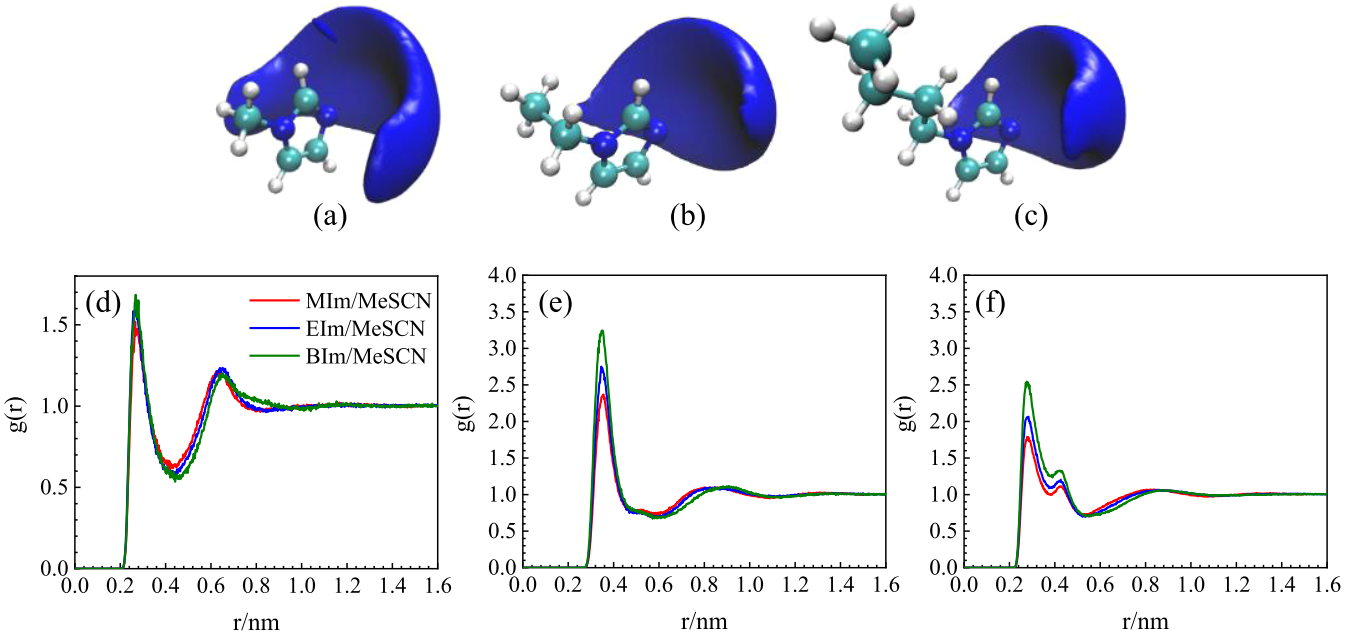

Figure 5. SDF of MeSCN around alkylimidazole in different systems (a) MIm/MeSCN, (b) EIm/MeSCN, and (c) BIm/MeSCN, and RDFs between the H5 of imidazole and the N1 of MeSCN (d), the N2 of imidazole and the CS of MeSCN (e), and the N2 of imidazole and the HC of MeSCN (f) in different systems with the labels shown in Figure 1.

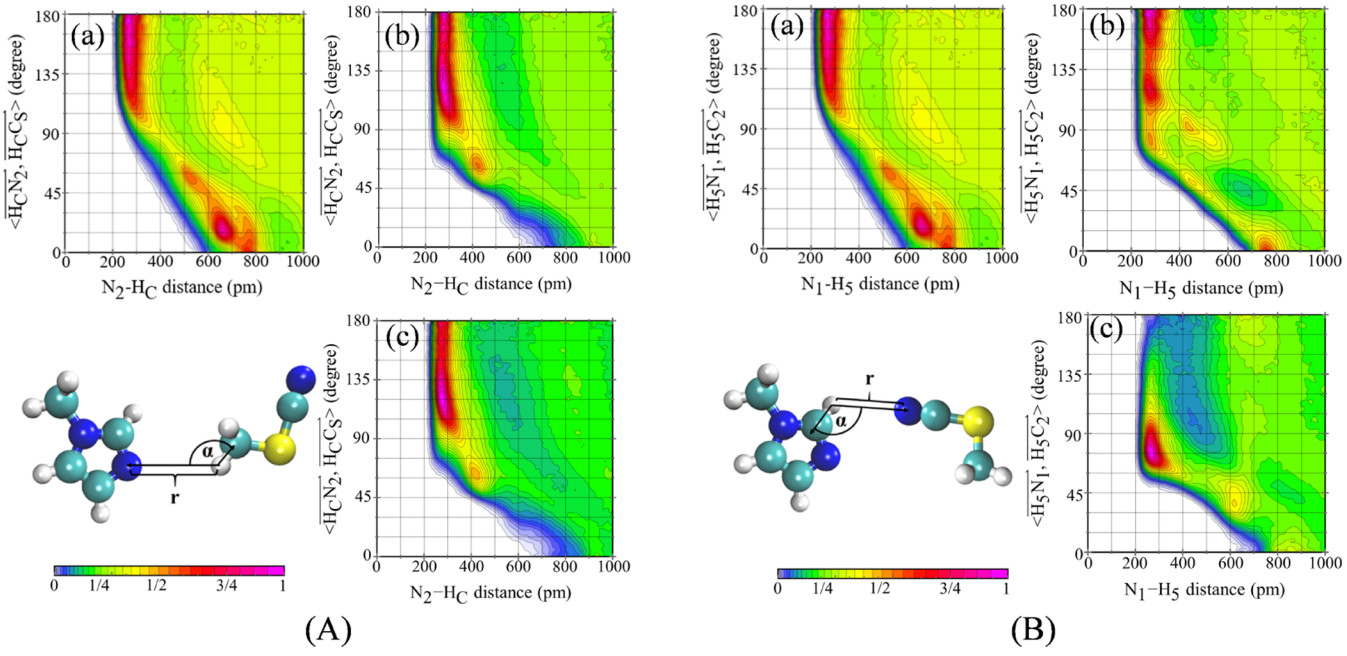

Figure 6. Distance-angle distributions of the N2 atom and HC atom in (a) MIm/MeSCN, (b) EIm/MeSCN, and (c) BIm/MeSCN systems in panel (A), and the distance-angle distributions of the N1 atom and H5 atom in (a) MIm/MeSCN, (b) EIm/MeSCN, and (c) BIm/MeSCN systems in panel (B)

the increased activation energy caused by alkylimidazole with a longer alkyl chain. For comparison, the activation energies of the MIm/MeSCN, MIm/EtSCN, and MIm/BuSCN systems are 65.8, 85.4, and 93.3 kJ/mol, respectively, as reported in our previous work.[20] Thus, compared to the change of activation energy with a prolonged alkyl chain of imidazole, it is much smaller than that of the alkylthiocyanate substrate with the same substituent. Thus, the alkyl chain length of the imidazole nucleophile shows a less important effect compared to that of the alkylthiocyanate substrate for the synthesis of imidazolium thiocyanate-based ILs.

3.3. Microstructure. To further probe the alkyl chain of imidazole on the microstructure of the reaction system, the spatial distribution function (SDF) and radical distribution function (RDF) in different systems are calculated using the *TRAVIS* package. The SDF of MeSCN around alkylimidazole in different systems is displayed in Figure 5. In the MIm/MeSCN system, MeSCN molecules tend to distribute around the N2 atom of the methylimidazole and on the plane

https://doi.org/10.1021/acs.iecr.3c01512
Ind. Eng. Chem. Res. 2023, 62, 14963−14972

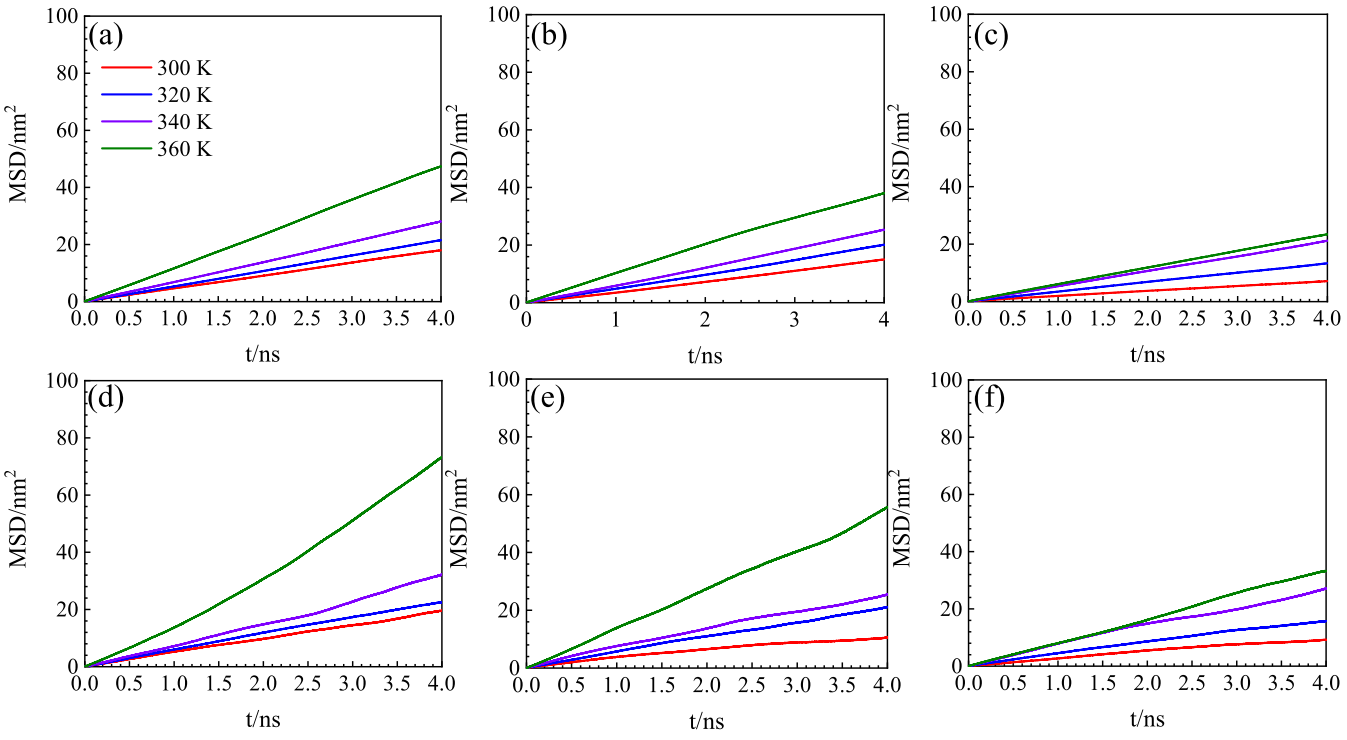

Figure 7. MSD curves of alkylimidazole and MeSCN in the MIm/MeSCN (a, d), EIm/MeSCN (b, e), and BIm/MeSCN (c, f) systems at different temperatures.

perpendicular to the imidazole ring, while the distribution of MeSCN near the methyl group of imidazole far from the reaction site is rare. With the increased alkyl chain length of the imidazolium, the distribution of MeSCN becomes more enriched around the N2 atom of the alkylimidazole, and the probability of distribution of MeSCN perpendicular to the imidazole ring drops. This indicates that the increase in the alkyl chain length of imidazole leads to a decrease in distribution near the alkyl chain and a more concentrated distribution around the reaction site.

To examine the impact of the alkyl chain length of alkylimidazole on the microstructure characteristics of the reaction system, Figure 5 also presents the atom−atom RDF*s* between imidazole and MeSCN. Figure 5d displays the RDF*s* between the H5 atom of imidazole and the N1 atom of MeSCN. In all three systems, the first peak is located at approximately 0.266 nm and the peak intensity exceeds 1.5, indicating a strong hydrogen-bonding interaction. Furthermore, the intensity of the first peak moderately increases as the alkyl chain length of imidazole increases. Figure 5e shows the RDF between the N2 atom of imidazole and the CS atom of MeSCN. The first peaks of the RDF*s* in all three systems are situated at 0.352 nm, and the peak intensity surpasses that of H5−N1. Additionally, the peak intensity increases with the increase in the alkyl chain length of alkylimidazole. For instance, the first peak intensity of the RDF*s* in the MIm/MeSCN system is slightly greater than 2.3, whereas that in the BIm/MeSCN system exceeds 3. Similarly, in Figure 5f, the RDF between the N2 atom of imidazole and the HC atom of MeSCN displays the first peaks located at 0.278 nm, indicating the existence of the hydrogen-bonding interaction. As the alkyl chain length of imidazole increases, the first peak height of the RDFs between the N2 atom of imidazole and the HC atom of MeSCN increases. This suggests that MeSCN is inclined to concentrate at the reaction site of N2 with the increased alkyl chain length of imidazole, which is in good agreement with the SDF results.

3.4. Hydrogen-Bonding Interactions. To further analyze the hydrogen-bonding interaction between imidazole and MeSCN, the distance-angle distribution between the N2 atom of imidazole with different alkyl chain lengths and the HC atom of MeSCN was calculated, as shown in Figure 6A. The conventional hydrogen-bonding interaction is generally defined as N2−HC (or H5−N1) distance less than 0.35 nm and N2−HC−CS (or C2−H5−N1) angles greater than 150°. The Z-bonding, a novel and unique type of hydrogen bond, has the general structure of +[X−H···A]−, where X and A are electronegative atoms. The angle of the Z-bond always ranges from 120 to 150°, which is bent in comparison with a hydrogen bond. The $d_{H\cdots A}$ bond is longer than that of a conventional hydrogen bond due to the nonlocal charge distribution in the cation or anion.[40] From Figure 6A, there is a higher probability of the N2−HC distance being distributed at less than 0.35 nm, with the N2−HC−CS angle in the range of 135−180° in the first solvation shell for the MIm/MeSCN system, indicating the presence of conventional hydrogen bonds and Z-bonds between the N2 atom of MIm and HC of MeSCN. However, the high probability distribution of N2−HC at a distance of 0.65−0.7 nm with N2−HC−CS angles less than 30° is also observed, which indicates the higher distribution of MeSCN around MIm in the second solvation shell, corresponding to the results in Figure 5d. In addition, the N2−HC distance distributed at less than 0.35 nm with the N2−HC−CS angle around 120° indicates the strong Z-bond in the EIm/MeSCN and BIm/MeSCN systems.

The distance-angle distribution between the N1 atom of MeSCN and the H5 atom of imidazole with different alkyl chain lengths was further analyzed, as shown in Figure 6B. In

https://doi.org/10.1021/acs.iecr.3c01512
Ind. Eng. Chem. Res. 2023, 62, 14963−14972

Table 2. Temperature-Dependent Self-Diffusion Coefficients in Different Systems

	MIm/MeSCN		EIm/MeSCN		BIm/MeSCN	
temperature (K)	$D_{MIm} \times 10^9$ (m^2/s)	$D_{MeSCN} \times 10^9$ (m^2/s)	$D_{EIm} \times 10^9$ (m^2/s)	$D_{MeSCN} \times 10^9$ (m^2/s)	$D_{BIm} \times 10^9$ (m^2/s)	$D_{MeSCN} \times 10^9$ (m^2/s)
300	0.467	0.526	0.349	0.388	0.204	0.270
320	0.548	0.601	0.487	0.574	0.352	0.458
340	0.724	0.739	0.589	0.703	0.541	0.692
360	1.256	1.308	1.032	1.084	0.615	0.809

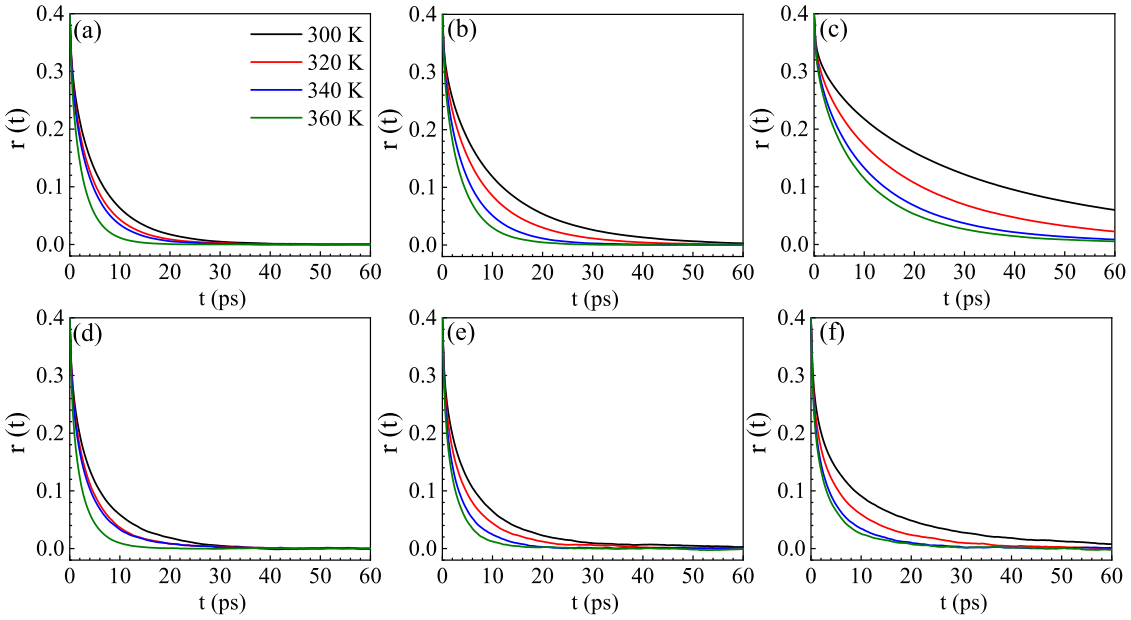

Figure 8. Reorientation of imidazole and MeSCN in the MIm/MeSCN (a and d), EIm/MeSCN (b and e), and BIm/MeSCN (c and f) systems at different temperatures.

the MIm/MeSCN system and EIm/MeSCN system, the N1−H5 distance was located less than 0.35 nm, and the N1−H5−C2 angle has a higher probability with a value greater than 150°, suggesting the presence of the hydrogen-bonding interaction between H5 of MIm and N1 of MeSCN. In the BIm/MeSCN system, however, there is a higher probability distribution within N1−H5 distances less than 0.3 nm and N1−H5−C2 angles between 60 and 90°, indicating that BIm does not form conventional hydrogen bonding with MeSCN through the N1−H5 atom. To sum up, the increase in the alkyl chain length of imidazole has a significant effect on the formation of conventional hydrogen bonds and Z-bonds between H5 of imidazole and N1 of MeSCN, probably due to the increased steric hindrance, which affects the spatial distribution of MeSCN molecules near imidazole and the formation of hydrogen bonds.

3.5. Microdynamics. The mean-squared displacement (MSD) of MIm, EIm, BIm, and MeSCN as a function of time is calculated using the following equation to study the effect of the alkyl chain length of imidazole on the microdynamics

$$\mathrm{MSD} = \langle |x(t) - x(0)|^2 \rangle = \frac{1}{N} \sum_{i=1}^{N} |x_i(t) - x_i(0)|^2 = t^{\beta} \tag{10}$$

where β describes the mode of motion. According to the Einstein equation, the self-diffusion coefficient (D) was obtained by the slope of the MSD−t curve

$$D = \frac{1}{6} \lim_{\Delta t \to \infty} \frac{\mathrm{dMSD}}{\mathrm{d}\Delta t} \tag{11}$$

The MSDs of alkylimidazole and MeSCN of all of the systems at different temperatures are linearly dependent on time, as shown in Figure 7. The corresponding self-diffusion coefficients of alkylimidazole and MeSCN in different systems are presented in Table 2. It is clear that the Ds of alkylimidazole and MeSCN increase with temperature for all of the systems. However, as the alkyl chain length of imidazole increases, the Ds of alkylimidazole and MeSCN decrease at the same temperature. For example, the D of MIm and MeSCN is 1.256×10^{-9} and 1.308×10^{-9} m^2/s, respectively, in the MIm/MeSCN system at 360 K. In the BIm/MeSCN system, the D of BIm and MeSCN is 0.651×10^{-9} and 0.809×10^{-9} m^2/s, respectively. When the branched chain of imidazole changes from methyl to butyl, the D of alkylimidazole decreases by a factor of 2, while the D of MeSCN decreases by a factor of 1.6. Thus, the increased alkyl chain length of imidazole significantly affects the diffusion behaviors of alkylimidazole and MeSCN in different systems, particularly on the diffusion of alkylimidazole molecules themselves.

To further describe the dynamics of alkylimidazole and MeSCN molecules in different systems, the rotational dynamics of the molecules was calculated using the following equation

$$r(t) = \frac{2}{5} C_2(t) = \frac{2}{5} \langle P_2[\vec{e}(t) \cdot \vec{e}(0)] \rangle \tag{12}$$

https://doi.org/10.1021/acs.iecr.3c01512
Ind. Eng. Chem. Res. 2023, 62, 14963−14972

where $C_2(t)$ is the direction-correlation function obtained from MD simulations, P2 is the second-order Legendre polynomial, and $\vec{e}(t)$ is the unit vector of the transition dipole moment at time t.

Figure 8 shows the rotational dynamics ($r(t)$) of the N−N bond of alkylimidazole and the C−N bond of MeSCN at different temperatures from 300 to 360 K. As the temperature increases, the decay time of $r(t)$ for both alkylimidazole and MeSCN becomes significantly slower, indicating faster rotational dynamics of the molecules at higher temperatures. At the same temperature, as the alkyl chain length of alkylimidazole increases, the $r(t)$ slows and the decay time becomes longer. The $r(t)$ of MeSCN follows a trend similar to that of alkylimidazole. From Figure 8a−c, the N−N bond of the MIm/MeSCN system decays to zero within 30−40 ps, while the N−N bond of the EIm/MeSCN system takes 60 ps, and the N−N bond in the BIm/MeSCN system takes more than 60 ps at low temperature. Similarly, comparing Figure 8d−f, the decay of MeSCN also becomes slower with the increased alkyl chain length of imidazole.

The reorientation dynamics of MIm, EIm, BIm, and MeSCN are well described by a double exponential fitting, and the corresponding parameters are listed in Tables S2−S4. The comparison of the reorientation dynamics parameters of MIm, EIm, BIm, and MeSCN at 300 K is given in Table 3. It can be

Table 3. Orientational Relaxation Parameters in MIm/MeSCN, MIm/EtSCN, and MIm/BuSCN Systems at 300 K

system	species	A_1	t_1 (ps)	A_2	t_2 (ps)	τ_c (ps)
MIm/MeSCN	MIm-NN	0.127	0.736	0.266	7.074	2.002
	MeSCN-CN	0.161	0.862	0.229	7.516	1.860
BIm/MeSCN	MIm-NN	0.109	0.920	0.277	11.652	3.522
	EtSCN-CN	0.155	0.703	0.232	7.454	2.149
BIm/MeSCN	MIm-NN	0.080	0.976	0.271	25.451	8.531
	BuSCN-CN	0.182	0.891	0.194	12.084	3.100

seen that an increase in the temperature results in smaller first (t_1) and second (t_2) time scales. As the length of the imidazolium alkyl chain increases, the amplitude A_1 of the imidazolium decreases, while that of MeSCN increases. The values of t_1 and t_2 for imidazolium increase with the length of the alkyl chain, which indicates that t_1 and t_2 are sensitive to steric hindrance. In addition, the integral correlation time (τ_c) was calculated using eq 13

$$\tau_c = \frac{1}{A(0)} \int_0^\infty A(t)\mathrm{d}t \tag{13}$$

where $A(t)/A(0)$ represents the normalized correlation function. In the same system, τ_c decreases for both alkylimidazole and MeSCN as the temperature increases. At the same temperature, τ_c increases for both alkylimidazole and MeSCN as the alkyl chain length increases. The τ_c value for BIm is approximately 4.25 times greater than that of MIm at 300 K, whereas the τ_c value for MeSCN in the BIm/MeSCN system is only 1.67 times greater than that in the MIm/MeSCN system. Therefore, the alkyl chain length of imidazole can slow down the diffusion and reorientation dynamics of reactant molecules, mainly due to the increased steric hindrance, which can reduce the intermolecular collision probability and further reduce the reaction rate.

4. CONCLUSIONS

The reaction kinetics, microstructure, and microdynamic behaviors of Menshutkin SN2 reactions between imidazole with different alkyl chain lengths and MeSCN were investigated using FTIR and MD simulations. The longer alkyl chain length of imidazole is found to decrease the reaction rate, and the activation energy of the BIm/MeSCN system is 8.3 kJ/mol higher than that of the MIm/MeSCN system. From MD simulations, the longer alkyl chain length of imidazole results in a larger spatial distribution near the imidazole N1 atom, leading to a more concentrated distribution of MeSCN near the N2 atom. As the alkyl chain length of imidazole increases, the Ds of alkylimidazole and MeSCN gradually decrease. According to the $r(t)$ results, the decay time of BIm molecules in the BIm/MeSCN system is significantly slower than that of MIm molecules in the MIm/MeSCN system, indicating that the increased alkyl chain length of imidazole can slow down the molecular motion of the reaction systems, and accordingly, the probability of molecular collisions is decreased. The work can provide guidance for the preparation of imidazolium-based ILs with different alkyl chain lengths industrially.

■ ASSOCIATED CONTENT

Supporting Information

The Supporting Information is available free of charge at https://pubs.acs.org/doi/10.1021/acs.iecr.3c01512.

Detailed results of density and orientational relaxation parameters of the MIm, EIm, BIm, and MeSCN (PDF)

■ AUTHOR INFORMATION

Corresponding Authors

Weizhen Sun − *State Key Laboratory of Chemical Engineering, School of Chemical Engineering, East China University of Science and Technology, Shanghai 200237, China;* orcid.org/0000-0002-9957-3620; Email: sunwz@ecust.edu.cn

Ling Zhao − *State Key Laboratory of Chemical Engineering, School of Chemical Engineering, East China University of Science and Technology, Shanghai 200237, China;* orcid.org/0000-0001-5239-1152; Email: zhaoling@ecust.edu.cn

Authors

Weizhong Zheng − *State Key Laboratory of Chemical Engineering, School of Chemical Engineering, East China University of Science and Technology, Shanghai 200237, China;* orcid.org/0000-0002-3866-4932

Fan Zhang − *State Key Laboratory of Chemical Engineering, School of Chemical Engineering, East China University of Science and Technology, Shanghai 200237, China*

Fan Yang − *State Key Laboratory of Chemical Engineering, School of Chemical Engineering, East China University of Science and Technology, Shanghai 200237, China*

Complete contact information is available at: https://pubs.acs.org/10.1021/acs.iecr.3c01512

Notes

The authors declare no competing financial interest.

https://doi.org/10.1021/acs.iecr.3c01512
Ind. Eng. Chem. Res. 2023, 62, 14963−14972

■ ACKNOWLEDGMENTS

The financial support from the National Natural Science Foundation of China (22008065 and 91434108) is gratefully acknowledged.

■ REFERENCES

(1) Li, M.; Chen, J.; Li, L.; Ye, C.; Lin, X.; Qiu, T. Novel multi−SO_3H functionalized ionic liquids as highly efficient catalyst for synthesis of biodiesel. *Green Energy Environ.* **2021**, *6* (2), 271−282.
(2) Sun, W.; Wang, M.; Zhang, Y.; Ding, W.; Huo, F.; Wei, L.; He, H. Protic vs aprotic ionic liquid for CO_2 fixation: A simulation study. *Green Energy Environ.* **2020**, *5* (2), 183−194.
(3) Ghandi, K. A review of ionic liquids, their limits and applications. *Green Sustainable Chem.* **2014**, *04* (1), 44−53.
(4) Marsh, K. N.; Boxall, J. A.; Lichtenthaler, R. Room temperature ionic liquids and their mixtures—a review. *Fluid Phase Equilib.* **2004**, *219* (1), 93−98.
(5) Freemantle, M. *An Introduction to Ionic Liquids*; Royal Society of Chemistry, 2010.
(6) Nieto de Castro, C. A.; Langa, E.; Morais, A. L.; Lopes, M. L. M.; Lourenço, M. J.; Santos, F. J.; Santos, M. S. C.; Lopes, J. N. C.; Veiga, H. I.; Macatrão, M.; et al. Studies on the density, heat capacity, surface tension and infinite dilution diffusion with the ionic liquids $[C_4mim][NTf_2]$,$[C_4mim][dca]$,$[C_2mim][EtOSO_3]$ and [Aliquat]-[dca]. *Fluid Phase Equilib.* **2010**, *294* (1−2), 157−179.
(7) Bica, K.; Deetlefs, M.; Schröder, C.; Seddon, K. R. Polarisabilities of alkylimidazolium ionic liquids. *Phys. Chem. Chem. Phys.* **2013**, *15* (8), 2703−2711.
(8) Law, G.; Watson, P. R. Surface tension measurements of N-alkylimidazolium ionic liquids. *Langmuir* **2001**, *17* (20), 6138−6141.
(9) Bhat, M. A.; Dutta, C. K.; Rather, G. M. Exploring physicochemical aspects of N-alkylimidazolium based ionic liquids. *J. Mol. Liq.* **2013**, *181*, 142−151.
(10) Rocha, M. A. A.; AA, R. M.; Neves, C. M. S. S.; MSS, N. C.; Freire, M. G.; Olga, R.; Russina, O.; Alessandro, T.; Triolo, A.; AP, C. J. o.; Coutinho, J. A. P.; MNBF, S. L. s. Alkylimidazolium Based Ionic Liquids: Impact of Cation Symmetry on Their Nanoscale Structural Organization. *J. Phys. Chem. B* **2013**, *117*, 10889−10897.
(11) Kamavaram, V.; Reddy, R. G. Thermal stabilities of di-alkylimidazolium chloride ionic liquids. *Int. J. Thermal Sci.* **2008**, *47* (6), 773−777.
(12) Su, W. C.; Chou, C. H.; Wong, D. S. H.; Li, M. H. Diffusion coefficients and conductivities of alkylimidazolium tetrafluoroborates and hexafluorophosphates. *Fluid Phase Equilib.* **2007**, *252* (1−2), 74−78.
(13) Wu, J.; Zhang, L.; Long, J.; Zeng, Q.; Yin, B.; Li, X. Synthesis and fluorescent properties of quinoxaline derived ionic liquids. *Green Energy Environ.* **2022**, *7* (5), 996−1005.
(14) Yuan, X.; Liu, J.; Qin, J.; Ma, W.; Liu, G.; Wang, Y.; He, H. Smart ionic liquid/water mixture system with dual stimuli-response to temperature and CO_2. *Nano Res.* **2023**, *16* (3), 4152−4159.
(15) Wasserscheid, P.; Welton, T. *Ionic Liquids in Synthesis*; Wiley Online Library, 2008; Vol. *1*.
(16) Lerch, S.; Strassner, T. Synthesis and Physical Properties of Tunable Aryl Alkyl Ionic Liquids (TAAILs). *Chem. - Eur. J.* **2021**, *27* (62), 15554−15557.
(17) Schleicher, J. C.; Scurto, A. M. Kinetics and solvent effects in the synthesis of ionic liquids: imidazolium. *Green Chem.* **2009**, *11* (5), 694−703.
(18) Große Böwing, A.; Jess, A. Kinetics and reactor design aspects of the synthesis of ionic liquids—Experimental and theoretical studies for ethylmethylimidazole ethylsulfate. *Chem. Eng. Sci.* **2007**, *62* (6), 1760−1769.
(19) Appetecchi, G. B.; Montanino, M.; Zane, D.; Carewska, M.; Alessandrini, F.; Passerini, S. Effect of the alkyl group on the synthesis and the electrochemical properties of N-alkyl-N-methyl-pyrrolidinium bis (trifluoromethanesulfonyl) imide ionic liquids. *Electrochim. Acta* **2009**, *54* (4), 1325−1332.
(20) Zhang, F.; Zheng, W.; Yang, F.; Ma, Z.; Sun, W.; Zhao, L. Understanding the Reaction Kinetics and Microdynamics between Methylimidazole and Alkyl Thiocyanate for Ionic Liquid Synthesis through Experiments and Theoretical Calculation. *Ind. Eng. Chem. Res.* **2023**, *62* (9), 3889−3897.
(21) Bedrov, D.; Piquemal, J.-P.; Borodin, O.; MacKerell, A. D., Jr; Roux, B.; Schröder, C. Molecular dynamics simulations of ionic liquids and electrolytes using polarizable force fields. *Chem. Rev.* **2019**, *119* (13), 7940−7995.
(22) Neumann, J.; Golub, B.; Odebrecht, L.-M.; Ludwig, R.; Paschek, D. Revisiting imidazolium based ionic liquids: Effect of the conformation bias of the $[ntf_2]$ anion studied by molecular dynamics simulations. *J. Chem. Phys.* **2018**, *148* (19), No. 193828.
(23) Campetella, M.; Le Donne, A.; Daniele, M.; Gontrani, L.; Lupi, S.; Bodo, E.; Leonelli, F. Hydrogen bonding features in cholinium-based protic ionic liquids from molecular dynamics simulations. *J. Phys. Chem. B* **2018**, *122* (9), 2635−2645.
(24) Le Crom, S.; Dourdain, S.; Pellet-Rostaing, S.; Duvail, M. Long-range organization study of piperidinium-based ionic liquids by polarizable molecular dynamics simulations. *J. Phys. Chem. B* **2022**, *126* (17), 3355−3365.
(25) Brehm, M.; Weber, H.; Pensado, A. S.; Stark, A.; Kirchner, B. Proton transfer and polarity changes in ionic liquid−water mixtures: A perspective on hydrogen bonds from ab initio molecular dynamics at the example of 1-ethyl-3-methylimidazolium acetate−water mixtures—Part 1. *Phys. Chem. Chem. Phys.* **2012**, *14* (15), 5030−5044.
(26) Konieczny, J. K.; Szefczyk, B. Structure of Alkylimidazolium-Based Ionic Liquids at the Interface with Vacuum and Water— A Molecular Dynamics Study. *J. Phys. Chem. B* **2015**, *119* (9), 3795−3807.
(27) Gao, L.; Wan, H.; Han, M.; Guan, G. Deep desulfurization of model oil by extraction with a low-viscosity ionic liquid [BMIM]SCN. *Pet. Sci. Technol.* **2014**, *32* (11), 1309−1317.
(28) Li, A.; Xu, X.; Zhang, L.; Gao, J.; Xu, D.; Wang, Y. Separation of cresol from coal tar by imidazolium-based ionic liquid [Emim]-[SCN]: Interaction exploration and extraction experiment. *Fuel* **2020**, *264*, No. 116908.
(29) Corrales-Luna, M.; Le Manh, T.; Romero-Romo, M.; Palomar-Pardavé, M.; Arce-Estrada, E. M. 1-Ethyl 3-methylimidazolium thiocyanate ionic liquid as corrosion inhibitor of API 5L X52 steel in H_2SO_4 and HCl media. *Corros. Sci.* **2019**, *153*, 85−99.
(30) Zheng, W.; Yamada, S. A.; Hung, S. T.; Sun, W.; Zhao, L.; Fayer, M. D. Enhanced menshutkin SN2 reactivity in mesoporous silica: the influence of surface catalysis and confinement. *J. Am. Chem. Soc.* **2020**, *142* (12), 5636−5648.
(31) Martínez, L.; Andrade, R.; Birgin, E. G.; Martínez, J. M. PACKMOL: A package for building initial configurations for molecular dynamics simulations. *J. Comput. Chem.* **2009**, *30* (13), 2157−2164.
(32) Nosé, S. A unified formulation of the constant temperature molecular dynamics methods. *J. Chem. Phys.* **1984**, *81* (1), 511−519.
(33) Hoover, W. G. Canonical dynamics: Equilibrium phase-space distributions. *Phys. Rev. A* **1985**, *31* (3), 1695.
(34) Parrinello, M.; Rahman, A. Polymorphic transitions in single crystals: A new molecular dynamics method. *J. Appl. Phys.* **1981**, *52* (12), 7182−7190.
(35) Nosé, S.; Klein, M. Constant pressure molecular dynamics for molecular systems. *Mol. Phys.* **1983**, *50* (5), 1055−1076.
(36) Frisch, M.; Trucks, G.; Schlegel, H.; Scuseria, G.; Robb, M.; Cheeseman, J.; Scalmani, G.; Barone, V.; Mennucci, B.; Petersson, G. *Gaussian 09*, Revision D. 01; Gaussian, Inc.: Wallingford CT, 2009. See also: URL: http://www.gaussian.com.
(37) Van Der Spoel, D.; Lindahl, E.; Hess, B.; Groenhof, G.; Mark, A. E.; Berendsen, H. J. GROMACS: fast, flexible, and free. *J. Comput. Chem.* **2005**, *26* (16), 1701−1718.
(38) Hess, B.; Kutzner, C.; Van Der Spoel, D.; Lindahl, E. GROMACS 4: algorithms for highly efficient, load-balanced, and scalable molecular simulation. *J. Chem. Theory Comput.* **2008**, *4* (3), 435−447.

https://doi.org/10.1021/acs.iecr.3c01512
Ind. Eng. Chem. Res. 2023, 62, 14963−14972

(39) Sanchora, P.; Pandey, D. K.; Kagdada, H. L.; Materny, A.; Singh, D. K. Impact of alkyl chain length and water on the structure and properties of 1-alkyl-3-methylimidazolium chloride ionic liquids. *Phys. Chem. Chem. Phys.* **2020**, *22* (31), 17687−17704.
(40) Wang, Y.; He, H.; Wang, C.; Lu, Y.; Dong, K.; Huo, F.; Zhang, S. Insights into ionic liquids: From Z-bonds to quasi-liquids. *JACS Au* **2022**, *2* (3), 543−561.

https://doi.org/10.1021/acs.iecr.3c01512
Ind. Eng. Chem. Res. 2023, 62, 14963−14972